| ARAŞTIRMA MAKALESİ | RESEARCH ARTICLE |
|---|---|

## In Silico Phylogeny, Sequence and Structure Analyses of Fungal Thermoacidophilic GH11 Xylanases

## Fungal Termoasidofilik GH11 Ksilanazlarının *İn Siliko* Filojeni, Dizi ve Yapı Analizleri

**Yusuf SÜRMELİ[1*]**

## Abstract

Thermoacidophilic xylanase enzymes are mostly preferred for use as animal feed additives. In this study, we performed *in silico* phylogeny, sequence, structure, and enzyme-docked complex analyses of six thermoacidophilic GH11 xylanases belonging to various fungal species (*Gymnopus androsaceus* xylanase = *Ga*Xyl, *Penicilliopsis zonata* xylanase = *Pz*Xyl, *Aspergillus neoniger* xylanase = *An*Xyl, *Calocera viscosa* xylanase = *Cv*Xyl, *Acidomyces richmondensis* xylanase = *Ar*Xyl, *Oidiodendron maius* xylanase = *Om*Xyl). To do this, amino acid sequences of six fungal thermoacidophilic GH11 xylanases, belonging to unreviewed protein entries in the UniProt/TrEMBL database, were investigated at molecular phylogeny and amino acid sequence levels. In addition, three-dimensional predicted enzyme models were built and then validated by using various bioinformatics programs computationally. The interactions between enzyme and the substrate were analyzed via docking program in the presence of two substrates (xylotetraose = $X_4$ and xylopentaose = $X_5$). According to molecular phylogeny analysis, three clusters of these enzymes occurred: the first group had *Pz*Xyl, *An*Xyl, and *Cv*Xyl, and the second group possessed *Ga*Xyl and *Om*Xyl, and the third group included *Ar*Xyl. Multiple sequence alignment analysis demonstrated that the five xylanases (*Ar*Xyl, *Om*Xyl, *Cv*Xyl, *Pz*Xyl, *An*Xyl) had longer N-terminal regions, indicating greater thermal stability, relative to the *Ga*Xyl. Homology modeling showed that all the predicted model structures were, to a great extent, conserved. Docking analysis results indicated that *Cv*Xyl, *Om*Xyl, and *An*Xyl had higher binding efficiency to two substrates, compared to the *Ga*Xyl, *Pz*Xyl, and *Ar*Xyl xylanases, and *Cv*Xyl-$X_4$ docked complex had the highest substrate affinity with a binding energy of -9.8 kCal/mol. *Cv*Xyl, *Om*Xyl, and *An*Xyl enzymes commonly had arginine in B8 β-strand interacted with two substrates, different from the other enzymes having lower binding efficiency. As a result, it was concluded that the three thermoacidophilic xylanase enzymes might be better candidates as the animal feed additive.

**Keywords:** Thermoacidophilic xylanase, Molecular docking, GH11 xylanase, Animal feed additive, UniProt/TrEMBL database

[1*]**Sorumlu Yazar/Corresponding Author:** Yusuf Sürmeli, Department of Agricultural Biotechnology, Faculty of Agriculture, Tekirdağ Namık Kemal University, Tekirdağ, Turkey. E-mail: ysurmeli@gmail.com ⓘ OrcID: 0000-0002-9645-6314.

# Öz

Termoasidofilik ksilanaz enzimleri, çoğunlukla hayvan yemi katkı maddesi olarak tercih edilmektedir. Bu çalışmada, çeşitli mantar türlerine ait altı termoasidofilik GH11 ksilanazın (*Gymnopus androsaceus* ksilanazı = *Ga*Xyl, *Penicilliopsis zonata* ksilanazı = *Pz*Xyl, *Aspergillus neoniger* ksilanazı = *An*Xyl, *Calocera viscosa* ksilanazı = *Cv*Xyl, *Acidomyces richmondensis* ksilanazı = *Ar*Xyl, *Oidiodendron maius* ksilanazı = *Om*Xyl) *in siliko* filojeni, dizi, yapı ve enzim-docking kompleks analizleri gerçekleştirilmiştir. Bunu yapmak için, UniProt/TrEMBL veri tabanındaki gözden geçirilmemiş protein girdilerine ait altı mantar termoasidofilik GH11 ksilanazının amino asit dizileri moleküler filojeni ve dizi açısından araştırıldı. Ayrıca, üç boyutlu tahmini enzim modelleri oluşturuldu ve daha sonra çeşitli biyoinformatik programları kullanılarak hesaplamalı olarak doğrulandı. Enzim ve substrat arasındaki etkileşimler, iki substratın (ksilotetraoz = $X_4$ ve ksilopentaoz = $X_5$) varlığında docking programı aracılığıyla analiz edildi. Moleküler filojeni analizine göre, bu enzimlerin üç kümesi oluştu: birinci grup *Pz*Xyl, *An*Xyl ve *Cv*Xyl'e sahipti ve ikinci grup *Ga*Xyl ve *Om*Xyl'e sahipti ve üçüncü grup *Ar*Xyl'i içeriyordu. Çoklu dizi hizalama analizi, beş ksilanazın (*Ar*Xyl, *Om*Xyl, *Cv*Xyl, *Pz*Xyl, *An*Xyl) daha uzun N-terminal bölgelerine sahip olduğunu gösterdi, bu da *Ga*Xyl'e göre daha yüksek termal stabiliteye sahip olduklarını işaret etmiştir. Homoloji modelleme, tahmin edilen tüm model yapılarının büyük ölçüde korunduğunu gösterdi. Docking analizi sonuçları, *Cv*Xyl, *Om*Xyl ve *An*Xyl'in *Ga*Xyl, *Pz*Xyl ve *Ar*Xyl ksilanazlara kıyasla iki substrata daha yüksek bağlanma verimliliğine sahip olduğunu ve *Cv*Xyl-$X_4$ docking kompleksinin -9.8 kCal/mol'lük bir bağlanma enerjisiyle en yüksek substrat afinitesine sahip olduğunu gösterdi. *Cv*Xyl, *Om*Xyl ve *An*Xyl enzimleri, daha düşük bağlanma verimliliğine sahip diğer enzimlerden farklı olarak, yaygın olarak B8 β-kolunda iki substrat ile etkileşime giren arjinin içeriyordu. Sonuç olarak, bu üç termoasidofilik ksilanaz enziminin hayvan yemi katkı maddesi olarak daha iyi adaylar olabileceği sonucuna varılmıştır.

**Anahtar Kelimeler:** Termoasidofilik ksilanaz, Moleküler docking, GH11 ksilanaz, Hayvan yem katkısı, UniProt/TrEMBL veritabanı

## 1. Introduction

Endo-1,4-β-D-xylanases (E.C. 3.2.1.8) cleave the β-1,4-glycosidic bonds in the main chain of the xylan, which is a part of hemicellulose, the biggest portion of lignocellulosic material after cellulose (Nordberg Karlsson et al., 2018; Sánchez and Cardona, 2008; Wood et al., 1989). The xylanase enzymes are classified within seventeen glycoside hydrolase (GH) families (mainly GH10 and GH11), as indicated in the Carbohydrate Active Enzymes (CAZy) database (Drula et al., 2022) (http://www.cazy.org/) based on the resemblance of the structure of the active region and their sequences.

The xylanase enzyme market, annually estimated at 500 million US Dollars, has been growing for approximately 30 years (Bajpai, 1999; Kumar et al., 2017). In recent times, the xylanase enzymes are of big interest in many biotechnological areas including animal feed, biofuel, food, and pulp and paper industries (Beg et al., 2001; Chadha et al., 2019; Subramaniyan and Prema, 2002). GH11 xylanase enzymes are considered more favorable for many industrial processes (e.g. an improvement of animal feed digestibility) because they generally possess a bigger catalytic region, higher catalytic action, greater substrate specificity, and relatively small size facilitating the penetration into the fiber (Biely et al., 2016; Paës et al., 2012).

In fact, an addition of exogen enzyme (e.g. xylanase) into the animal feeds and the silage is one of the main strategy to increase the animal feed digestibility (Koçyiğit and Tüzemen, 2012; Park and Carey, 2019; Alagawany et al., 2018; Başkavak et al., 2008). The xylanase enzymes are expected to conserve most of the activity and stability in extreme conditions and therefore, xylanolytic extremozymes with great extreme stability and thermostability are favorable for the biotechnological fields including animal feed industry (Algan et al., 2021; Basu et al., 2018; Collins et al., 2005). Thermoacidophilic GH11 xylanase enzymes are helpful for a variety of industrial processes including an increase of animal feed digestibility, which is required for high temperature and acidic pH conditions, because of heat processes and passing in low pH areas of the digestive system (Ravindran, 2013; Smeets et al., 2014). However, most of the xylanolytic enzymes are not active under these extreme conditions (Boonyapakron et al., 2017; Collins et al., 2005; Xia and Wang, 2009). Comprehensive investigations of thermoacidophilic GH11 xylanase enzymes are in progress.

Microorganisms, particularly bacteria and fungi, are the most important sources of industrial xylanase enzymes (Beg et al., 2001; Motta et al., 2013). Fungi, rather than bacteria, mostly produce the industrial xylanase with thermoacidophilic aspect because they optimally work at acidic pH conditions (Chakdar et al., 2016). For example, a recent work has shown that thermoacidophilic xylanase enzyme of *Aspergillus tubingensis* possessed an optimum pH and temperature of 5.0 and 50°C, respectively (Intasit et al., 2022). In another study, Galanopoulou et al. (2021) have characterized thermophilic, acid-stable xylanase from *Byssochlamys spectabilis*, optimally working at 65°C and pH 3.5 (Galanopoulou et al., 2021).

As omics technologies have evolved, large volumes of fungal-derived whole genome sequences have quickly increased. In UniProt/TrEMBL database, these data-derived gene sequences are annotated as unreviewed sequences (The UniProt Consortium, 2021). In a recent study, it has been shown that 1302 unreviewed amino acid sequences of bacterial GH11 xylanase enzymes were available in UniProt/TrEMBL database (Sürmeli, 2022). Therefore, a broad range of sequences of unreviewed fungal thermoacidophilic GH11 xylanase enzyme may be acquired from UniProt/TrEMBL database. In this work, the investigation of the six fungal thermoacidophilic GH11 xylanases was carried out to determine their phylogenetical relatedness, amino acid sequence resemblance, the comparative aspects of their three-dimensional predicted structures, and the interactions with the substrates. For this purpose, the *in silico* analysis of the evolutionary relationship, multiple sequence alignment, the predicted homology model structures, and protein docking of the six fungal thermoacidophilic GH11 xylanase enzymes was carried out by utilizing the unreviewed and full-length amino acid sequences of these enzymes from the UniProt/TrEMBL database. The results acquired from the *in silico* analyses were confirmed and discussed with data of other experimental researches in literature.

## 2. Materials and Methods

### 2.1. Amino acid sequences of xylanases: the retrieval and selection

The sequences of unreviewed fungal GH11 xylanase enzymes were obtained from the UniProt/TrEMBL database (The UniProt Consortium, 2021). The sequences with the thermoacidophilic character were selected according to high melting temperature ($T_m$) by $T_m$ predictor program (Ku et al., 2009) and low isoelectric point (pI) by the ProtPram tool

(Gasteiger et al., 2005). The other biophysicochemical features (positively charged residues = PCR), threonine:serine ratio = T/S, and negatively charged residues = NCR), of the enzymes were detected via the ProtPram tool (Gasteiger et al., 2005). Among these enzymes, six fungal GH11 xylanases with the lowest pI were potentially accepted as thermoacidophilic enzymes, and they were used for the next analyses.

### 2.2. Molecular phylogeny and sequence analyses

The six fungal thermoacidophilic GH11 xylanases were analyzed at their molecular phylogeny and sequence levels. For doing this, phylogeny investigation was fulfilled using the maximum likelihood (ML) statistical technique having 500 bootstrap replications, and Jones-Taylor-Thornton (JTT) substitution model by MEGA11 software (Tamura et al., 2021). In addition, multiple sequence alignment was performed for comparison of their the xylanase sequences via Clustal Omega program (Madeira et al., 2019).

### 2.3. Homology modeling

The three-dimensional predicted model structures of fungal thermoacidophilic xylanases was carried out by ProMod3 software in SWISS-MODEL server (Mirdita et al., 2017; Steinegger et al., 2019; Studer et al., 2020; Studer et al., 2021). The validation of the six predicted models was performed by RaptorX (Wang et al., 2016). The models were evaluated at the overall and local quality levels and their Z-scores were determined via the ProSA server (Wiederstein and Sippl, 2007). Stereochemical qualities and dihedral angles of the 3D models were analyzed by ProCheck forming the Ramachandran plot (Laskowski et al., 1996). Also, Verify3D was used to predict the good match between the 3D models and their amino acid sequences compared with the known structures (Bowie et al., 1991). The Stride was applied to predict the secondary structures of the 3D models (Heinig and Frishman, 2004).

### 2.4. Molecular docking

The docking analysis of the six fungal thermoacidophilic xylanase enzymes was carried out to investigate the enzyme-substrate interactions on two different substrates (xylotetraose=$X_4$, and xylopentaose=$X_5$) by Autodock Vina (version 1.5.6) that uses the Lamarckian Genetic Algorithm (LGA) (Trott and Olson, 2010). To do this, the spatial data files (SDFs) belonging to the ligands were obtained using the PubChem database, and protein data bank (PDB) files were formed by PyMOL Molecular Graphics System (Version 2.0) (Schrödinger, LLC). Then, the substrate preparations for molecular docking were performed using Autodock Vina. The predicted model structures were also prepared for molecular docking by deleting the water molecules, adding the polar hydrogens, and selecting the Kollman atom charges. The grid values were fixed $90 \times 90 \times 90$ by a grid spacing of 0.375, and the other parameters were adjusted as default. Thus, nine poses were obtained for each enzyme-substrate docked complex. The pose of each docked complex with the highest binding affinity was used for the analysis of the protein-ligand interaction.

### 2.5. Data representation

The figures were represented using GraphPad Prism (version 6.00) for Windows (GraphPad Software, La Jolla, CA, USA) (www.graphpad.com), MEGA11 software, and PyMOL Molecular Graphics System (Version 2.0) (Schrödinger, LLC).

### 3. Results and Discussion

In the present work, *in silico* analysis of the six fungal thermoacidophilic GH11 xylanase enzymes was comparatively carried out to determine their evolutionary relationships, the similarities between their amino acid sequences, three-dimensional structure resemblance, and the interaction between the enzymes and ligands. To do this, the six amino acid sequences of the GH11 thermoacidophilic xylanase from various fungal species were chosen among 2584 UniProt/TrEMBL unreviewed entries, according to the high melting temperature $T_m$ (above 65°C), and low theoretical pI values. These six enzymes were *Gymnopus androsaceus* xylanases (*Ga*Xyl) (Barbi et al., 2020), *Penicilliopsis zonata* xylanase (*Pz*Xyl) (de Vries et al., 2017), *Aspergillus neoniger* xylanase (*An*Xyl) (The UniProt Consortium, 2021), *Calocera viscosa* xylanase (*Cv*Xyl) (Nagy et al., 2016), *Acidomyces richmondensis* (*Ar*Xyl) (Mosier et al., 2016), and *Oidiodendron maius* (*Om*Xyl) (The UniProt Consortium, 2021).

### 3.1. The determination of biophysicochemical properties of the enzymes

Biophysicochemical properties, such as theoretical pI value, a ratio of negatively charged residues to positively charged residues (NCR/PCR), and threonine:serine ratio (T/S), of the amino acid sequences of six enzymes were investigated by ProtParam tool (Gasteiger et al., 2005) as summarized in *Table 1*. The results indicated that the

theoretical pI values, a ratio of NCR/PCR and T/S of the xylanases were in a range of 3.64-4.16, 2.44-10.5 and 0.85-1.95, respectively (*Table 1*).

*Table 1. Some biophysicochemical properties of the thermoacidophilic xylanases*

| Protein ID | Protein name | Fungal source | Enzyme length (aa) | Molecular weight (kDa) | Theoretical pI | NCR/ PCR* | T/S |
|---|---|---|---|---|---|---|---|
| A0A6A4H8W9 | *Ga*Xyl | *Gymnopus androsaceus* | 185 | 19.62 | 3.64 | 10.5 | 0.94 |
| A0A1L9SJU9 | *Pz*Xyl | *Penicilliopsis zonata* | 213 | 23.56 | 3.86 | 4.57 | 0.85 |
| A0A318YH97 | *An*Xyl | *Aspergillus neoniger* | 231 | 24.84 | 3.92 | 3.4 | 1 |
| A0A167IM53 | *Cv*Xyl | *Calocera viscosa* | 225 | 23.95 | 4.13 | 2.62 | 1.95 |
| A0A150VDR5 | *Ar*Xyl | *Acidomyces richmondensis* | 215 | 23.23 | 4.13 | 2.62 | 1.33 |
| A0A0C3CZX7 | *Om*Xyl | *Oidiodendron maius* | 226 | 24.05 | 4.16 | 2.44 | 1.08 |

* NCR/PCR refers to a ratio of negatively charged residues to positively charged residues.

NCR/PCR and T/S, which are two biophysicochemical properties, might be clues for thermoacidophilic feature of the GH11 xylanases. Accordingly, the acidophilic property is characterized by a high number of acidic residues (glutamate and aspartate) on the enzyme surface and less number of PCR, which causes a high ratio of NCR/PCR (Fushinobu et al., 1998). For instance, the xylanase from *Neocallimastix patriciarum*, which works in an optimum pH of 5.8 (Pai et al., 2010), has an NCR/PCR ratio of 1.17 (*Figure S1*), whereas *Aspergillus niger* xylanase B, which possesses a 5.0 of optimum pH (Deng et al., 2006), has relatively a higher NCR/PCR ratio of 1.45 (*Figure S1*). Furthermore, a greater T/S ratio is an indicator of the thermostability of GH11 xylanase enzymes (Hakulinen et al., 2003). For instance, *Phanerochaete chrysosporium* xylanase (Decelle et al., 2004) and *Penicillium oxalicum* xylanase (Liao et al., 2012) optimally working at 60°C and 50°C had a T/S ratio of 0.85 and 0.52, respectively (*Figure S1*). Taken together, the present work proposed that the six GH11 xylanase enzymes might highly be thermoacidophiles.

### 3.2. The phylogenetic relationship and a comparison of the xylanase amino acid sequences

The molecular phylogeny of the six GH11 thermoacidophilic xylanases was analyzed with an output group, *Arabidopsis thaliana* beta-amylase amino acid sequence (Lao et al., 1999) by ML statistical technique in MEGA11 software. The results indicated that the enzymes can be evaluated as three different groups according to their closeness to the amino acid sequences: the first group included *Pz*Xyl, *An*Xyl, and *Cv*Xyl, the second group had *Ga*Xyl and *Om*Xyl, and the third group had only one member *Ar*Xyl, distant from the former two groups (*Figure 1*).

The multiple sequence alignment analysis results showed that each GH11 xylanase possessed various lengths of the N-terminal regions (NTRs). The five thermoacidophilic GH11 xylanase enzymes (*Ar*Xyl, *Om*Xyl, *Cv*Xyl, *Pz*Xyl, *An*Xyl) had a similar NTR size to each other and were clearly longer than *Ga*Xyl and Tx-xyl having similar NTR length (*Figure 2*). Tx-xyl, optimally working at 75°C and having a low molecular weight (20.6 kDa), was highly thermostable exhibiting a great $T_m$ above 12 h at 60°C (Debeire-Gosselin et al., 1992; Harris et al., 1994). In fact, the size of NTRs positively affects the thermostability of the GH11 xylanase enzymes (Han et al., 2017). Accordingly, GH11 xylanase enzymes of *Neocallimastix patriciarum and Nonomuraea flexuosa* possess large NTRs and high thermostability (Cheng et al., 2014; Hakulinen et al., 2003; Han et al., 2017). Amino acid replacements enhance the thermostability of these enzymes generally located at the NTRs (Turunen et al., 2001; Xiong et al., 2004). Recent work has shown that engineered N-terminal sequence resulted in an increase in thermal

stability of GH11 xylanase from *Talaromyces leycettanus* (Wang et al., 2017). The present work indicated that the five enzymes might have greater thermostability, relative to the *Ga*Xyl and Tx-xyl, which might possess a similar thermostability.
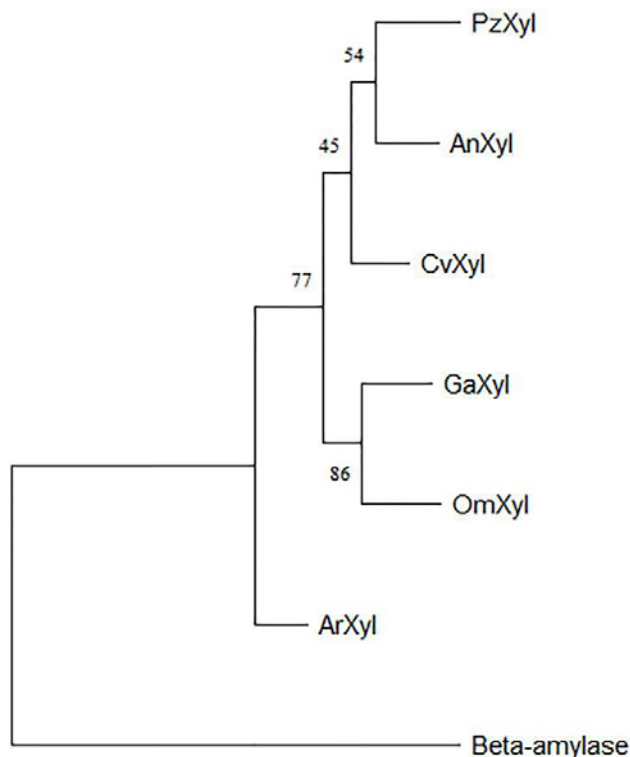


*Figure 1. The evolutionary relationship of the six thermoacidophilic fungal xylanase enzymes. Arabidopsis thaliana beta-amylase was used as output group.*



*Figure 2. The sequence alignment of the N-terminal sites of the six thermoacidophilic fungal xylanases, relative to the Tx-xyl.*

Paës et al. (2012) have shown that 17 residues from the GH11 xylanase active site are highly similar as a result of the structural investigation of the superimposed xylanase enzyme of *Thermobacillus xylanilyticus* (Tx-xyl). This work has also indicated that triple residues (P114-S115-I116) settled in the thumb site of the GH11 xylanase enzymes had a similarity of above 90% frequency, and I116 is occasionally substituted by valine or leucine. In addition, P88 from the active site is available in 80% of the enzyme amino acid sequences (Paës et al., 2012). The present work showed that the 11 amino acids in the thermoacidophilic enzymes such as catalytic residues

(acid/base and nucleophile residues), and serine-isoleucine of the triple residues were highly conserved in reference to Tx-xyl (*Figure 3*).

```
Tx-xyl   --------------------------------------------------NTYWQYWT      8
ArXyl    MYTKYITIL-VLATLSVVDAAPAV---------VNKRETI---TGSTSGTYDGYYFQNYV    47
OmXyl    MVALFNLVAILSAFAGS-LASPVDPATRNLAERGPADFVLGSENAVQRRQSTN-YDQDYT    58
GaXyl    -------------------------------------------------MAFSIPSLL      9
PzXyl    MKAF---LLSALATL-----------SLASA-PPAKRQI---TTSTTGTSDGWYYSFWT    41
AnXyl    MVAYSSLLLALSAASSA-VALPN----GKALL-DMAKRSL---TSSAEGESNGYFYSFWT    51
CvXyl    MVPFTSVFALVLAAAGI-LAAPTSLDKRQPTE-LAERQTI---TASQTGTNNGYYYQLWT    55


Tx-xyl   DGIGYVNATNGQGGNYSVSWSNS-GNFVIGKGWQYGAHNRVVNYNAGAWQPNGN--AYLT    65
ArXyl    ESGTGATLT-LNSNSYTLGWDSAAEDVVAGIGWNPGAER-DVTYS-ATVDWNGD--SLLA   102
OmXyl    -TGGDVIYT-PNGNSFTVDWDTE-DDFVVGVGWSTGNTS-PITFS-GSFGVGGG-TGLLS   112
GaXyl    LALPIVTFFTNIAGGDYEIQWDGS-GDFVVGQGANPGSTSAEITFG-GSFEPSADAAVILS    67
PzXyl    NGGGTVDYTNDDGGEYTVTWEDC-GDFTCGKGWEVGSER-DITFS-ADFSPSGN--AYLA    96
AnXyl    NGEGDVTYTNGDGGEYTVEWTDC-GDFVAGKGWNPGSAQ-AVTYS-GSWETDAN--AYLS   106
CvXyl    EGTGTVDYTNGAAGEYAVTWTDA-GDFTAGKGWATGSAR-AITFS-ATNVNLGT--GYLS   110
                   . *    ...: : *     :|.  * *  *       :.:. .       *:

Tx-xyl   LYSWTRNPLIEYYVVD--SWGSYRPT--GDYRGSVYSDGAWYDLYHSWRYNAPSIDG-TQ   120
ArXyl    LYGWTTNPLVEYYVIE--SYGTYNPGSAGTYKGSITSDGSTYVV----RYDAPSIEG-TS   155
OmXyl    VYGWTTSPLVEYYIIEDN----SSPPSFGTQKGTVTSDGATYTIWENQRVNEPSIEG-TS   167
GaXyl    VYGWSENPLVEYYINEFNNAGQFDLTFEATQVGTVTSDGSLYDIYLHQQVDQPSIEG-TA   126
PzXyl    VYSWTENPLIEYYILE--NYGDYDPGTEMTYMGSVESDGSLYYIYEHEQVDQPSVESDSS   154
AnXyl    VYGWTTSPLVEFYIVD--KYGDYDPSSGLTELGTVDSDDGTYKIYQTTREDADSIEG-TA   163
CvXyl    VYGWSTDPLVEFYIVE--DWAGYDPSSGGTYQGTLTSDGATYDVYEDTRTNEPSIEG-TA   167
         :.*|*|:. .**:|*|*|: :         *:: **.. * :       :|:. *:|:. :

Tx-xyl   TFQQYWSVRQQKRPTGSNVSITFENHVNAWGAAGMPMGSSWSYQVLATEGYYSSGYSNVT   180
ArXyl    TFNQYLSIRQNQRTSG---TITFSNHVQGWADVGMDLG-TWNLQIMATEGYESSGETIVT   211
OmXyl    TFNQYISVRQSPRTSG---TVTLENHQAWANLGLDLG-SFSYQVIAVEGWGGTGAATQT   223
GaXyl    TFNQYISVRQDERTSG---TVTVANHVNAWASLGLDLG-TLNYQIVAVEGLSGSGQATVT   182
PzXyl    TFMQYWSIRVDLRSEG---TVTTANHFAAWEELGMSLGSDFNYQIMLTEGYESSGSSIVT   211
AnXyl    TFKQYWSVRTEGRIGG---TVTTQNHFDAWENLGLDLG-TFNYMIVATEGYESSGSATIT   219
CvXyl    TFNQYWSVRQTTRTSG---TVTTANHFDAWASLGMNLG-TFNYQIVSTEGFGSSGSATVT   223
         ** |**|*:* * *    ::* **. .*   *: :*    . :: .|*|  .:* :  *

Tx-xyl   VW----------   182
ArXyl    VQGL--------   215
OmXyl    VSK---------   226
GaXyl    VDI---------   185
PzXyl    VS----------   213
AnXyl    VDTSSDSTEESC   231
CvXyl    VS----------   225
         *
```
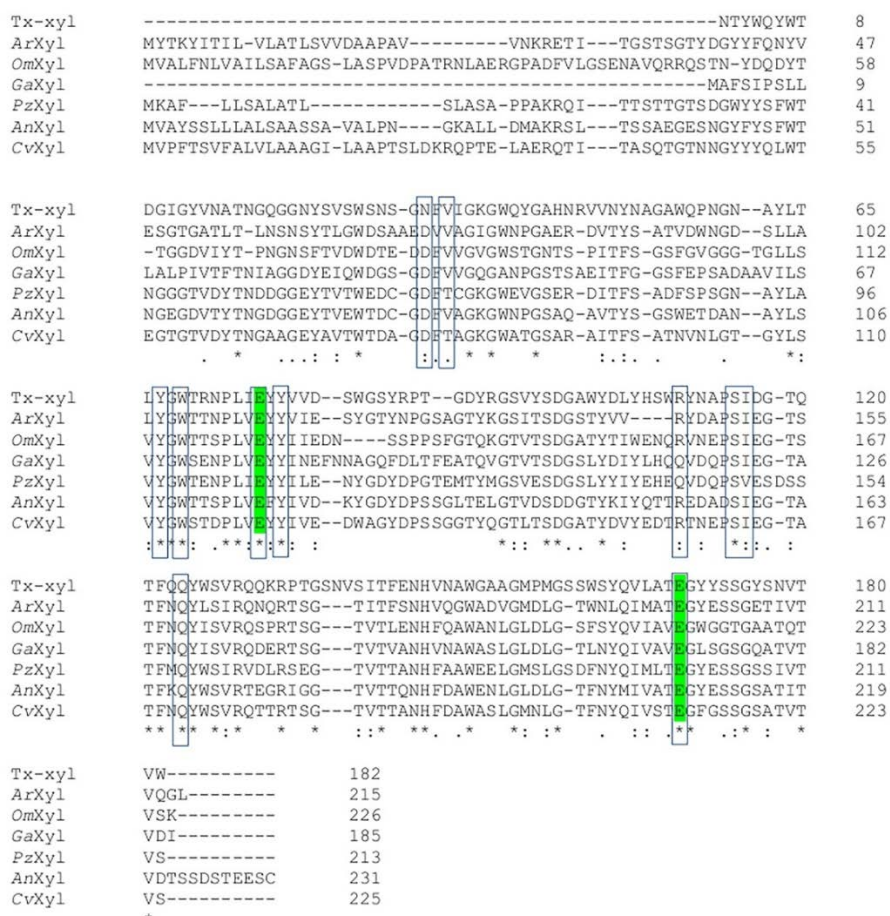
*Figure 3. The sequence alignment of the six thermoacidophilic enzymes, compared to the Tx-xyl. The highlighted amino acids show the conserved residues including catalytic amino acids with green highlighted amino acids.*

### 3.3. The predicted structures of thermoacidophilic xylanases

The predicted model structures of the six thermoacidophilic xylanases were determined via the SWISS-MODEL homology modeling server according to their sequences, and the validation of the structures was performed by

*Table 2. The modeling scores of three-dimensional predicted structures of the six thermoacidophilic enzymes and their template selections*

| No | Protein ID | Protein name | Template | Sequence identity (%) | Coverage (%) | GMQE | QMEAN | QMEAN Disco | Sequence similarity (%) |
|----|------------|--------------|----------|----------------------|--------------|------|-------|-------------|-------------------------|
| 1 | A0A6A4H8W9 | *Ga*Xyl | 6JWB | 56.55 | 91 | 0.84 | 0.59 | 0.83 ± 0.07 | 46 |
| 2 | A0A1L9SJU9 | *Pz*Xyl | 3WP3 | 62.83 | 90 | 0.84 | 0.01 | 0.87 ± 0.06 | 51 |
| 3 | A0A318YH97 | *An*Xyl | 3WP3 | 69.63 | 83 | 0.81 | 1.09 | 0.87 ± 0.06 | 53 |
| 4 | A0A167IM53 | *Cv*Xyl | 3WP3 | 62.24 | 87 | 0.81 | -0.52 | 0.86 ± 0.06 | 50 |
| 5 | A0A150VDR5 | *Ar*Xyl | 7EO6 | 51.35 | 86 | 0.77 | -1.05 | 0.76 ± 0.06 | 46 |
| 6 | A0A0C3CZX7 | *Om*Xyl | 1XYN | 71.75 | 78 | 0.78 | 0.36 | 0.91 ± 0.07 | 54 |

RaptorX. The template selection was carried out based on sequence identity, sequence similarity, the global model quality estimate (GMQE) value, and coverage.

The best template of the *Ga*Xyl was determined as 6JWB, chain 1A from *Trichoderma reesei* (Li et al., 2020) possessing a sequence identity of 56.55% and a coverage of 91%. In addition, the most convenient template of *Ar*Xyl was 7EO6, chain 1A of *Actinomycetia* bacterium (Yi et al., 2021) with 86% of coverage and 51.35% of sequence identity. As for *Om*Xyl, the best template was selected as 1XYN chain 1A of *Trichoderma reesei* (Törrönen and Rouvinen, 1995), having 71.75% and 78% of sequence identity and coverage, respectively. For the remaining three enzymes (*Pz*Xyl, *An*Xyl, *Cv*Xyl), the common template was selected as 3WP3, chain 1A of *Talaromyces cellulolyticus* (Kataoka et al., 2014) with a range of 62-69% and 83-90%, of sequence identity and coverage, respectively. Three quality parameters (GMQE, QMEAN, and QMEANDisCo values) showed that the predicted models had a high quality (*Table 2*).

The predicted models (*Figure S2*) built via SWISS-MODEL were validated by various bioinformatics tools. Regarding this, the secondary structures belonging to the predicted models were monitored in *Figure S3*. The 3D structure alignment indicated that each predicted model structure and its template had great compatibility and similarity in terms of overall and local structural patterns (*Figure S4*). Ramachandran plot analysis results indicated that most of the amino acids in the enzymes, with a range of 83.6%-91.9%, were found in the most favored regions. The enzymes *Ga*Xyl, *An*Xyl, *Ar*Xyl, and *Om*Xyl did not possess a Ramachandran outlier, but *Pz*Xyl and *Cv*Xyl had two outlier residues (*Figure S5*). As for the qualitative model energy analysis (QMEAN) scores, major geometrical features of the predicted models indicated that they had a high resemblance to the native structures giving the scores in the range of -1.05 to 1.09, around zero (*Figure S6*). Consideration of the predicted structures with three-dimensional profiles was performed by Verify 3D and the averaged 3D-1D score ≥ 0.2 was found as about 100% of the amino acids in structures of *An*Xyl, *Cv*Xyl, *Ar*Xyl, and *Om*Xyl. This score encompassed 97.09% and 90.1% of the residues for the structures of *Ga*Xyl and *Pz*Xyl, respectively (*Figure S7*). Also, the global quality of the predicted enzyme structures was considered by Z-scores obtained from the ProSA server. This analysis showed that all models except *Ar*Xyl (having -5.33) had an estimated Z score of above -6.0 (ranging from -6.01 to -6.91). These scores were intervals of the negative energy cut-off, validating the high quality of the predicted enzyme structures (*Figure S8*). The Z scores are estimated by a comparison of the Z-scores of the other existing structures of similar size, acquired using experimental techniques (e.g. X-ray and/or NMR).

The GH11 xylanase enzymes are structurally consisted of a β-jelly roll domain, which resembles a partially closed right hand. They have an α-helix and two-bent antiparallel β-sheets turning to each other and including 14 β-strands. One β-sheet constitutes five β-strands A2-A6, whereas another possesses nine β-strands B1-B9. Many (above 60%) of the residues are placed in two β-sheets and the α-helix (Paës et al., 2012; Törrönen et al., 1994). Also, the active cleft includes two grooves architectured with two β-sheets (Collins et al., 2005). The present work indicated that these structural characters were common in the six predicted model structures. Regarding this, *Pz*Xyl, *An*Xyl, *Cv*Xyl, and *Ar*Xyl possessed a full set of β-strands having an A4/B4-extended β-strand. Among these, *An*Xyl and *Ar*Xyl possessed one long A5 strand, whereas *Pz*Xyl and *Cv*Xyl had two small portions of this strand. On the other hand, *Ga*Xyl did not have A2 and B1 strands, whereas *Om*Xyl included no B1 strand (*Figure 4*).

### 3.4. The interactions between enzymes and the substrates

The docking analysis of the thermoacidophilic enzymes was carried out using xylotetraose ($X_4$) and xylopentaose ($X_5$) as the substrates and assessed the pose having the highest substrate affinity. The results indicated that *Cv*Xyl-$X_4$ docked complex possessed the highest substrate affinity with a binding energy of -9.8 kCal/mol, whereas $X_4$-docked complexes of *Ga*Xyl, *Pz*Xyl, and *Ar*Xyl had binding energy of -7.4 to -7.5 kCal/mol, having the lowest binding efficiency. In addition, *Cv*Xyl-$X_5$ docked complex had a binding energy of -8.9 kCal/mol with the greatest binding efficiency, whereas the smallest substrate efficiency belonged to *Ar*Xyl and *Ga*Xyl-$X_5$ docked complexes by a binding energy of -7.1 kCal/mol (*Table 3*).

The results of the analysis of protein-ligand interaction were shown in *Figure 5*. According to the results, the five common residues (T82 in B3-strand, Y206 in B4-strand, Y108 and Y112 in B5-strand, R157 in B8-strand) were involved in $X_4$ and $X_5$ substrate interactions in *Cv*Xyl. Similarly, corresponding residues in *Om*Xyl (Y206 in B4-strand, Y114 in B5-strand, and R157 in B8-strand), involved in the stabilization of *Cv*Xyl-docked complexes, could also form polar interactions with two substrates. In *An*Xyl, four residues (E208 in B4-strand, Y104 in B5-strand, T151 and R153 in B8-strand) might act on the stabilization of the *An*Xyl-docked complexes.
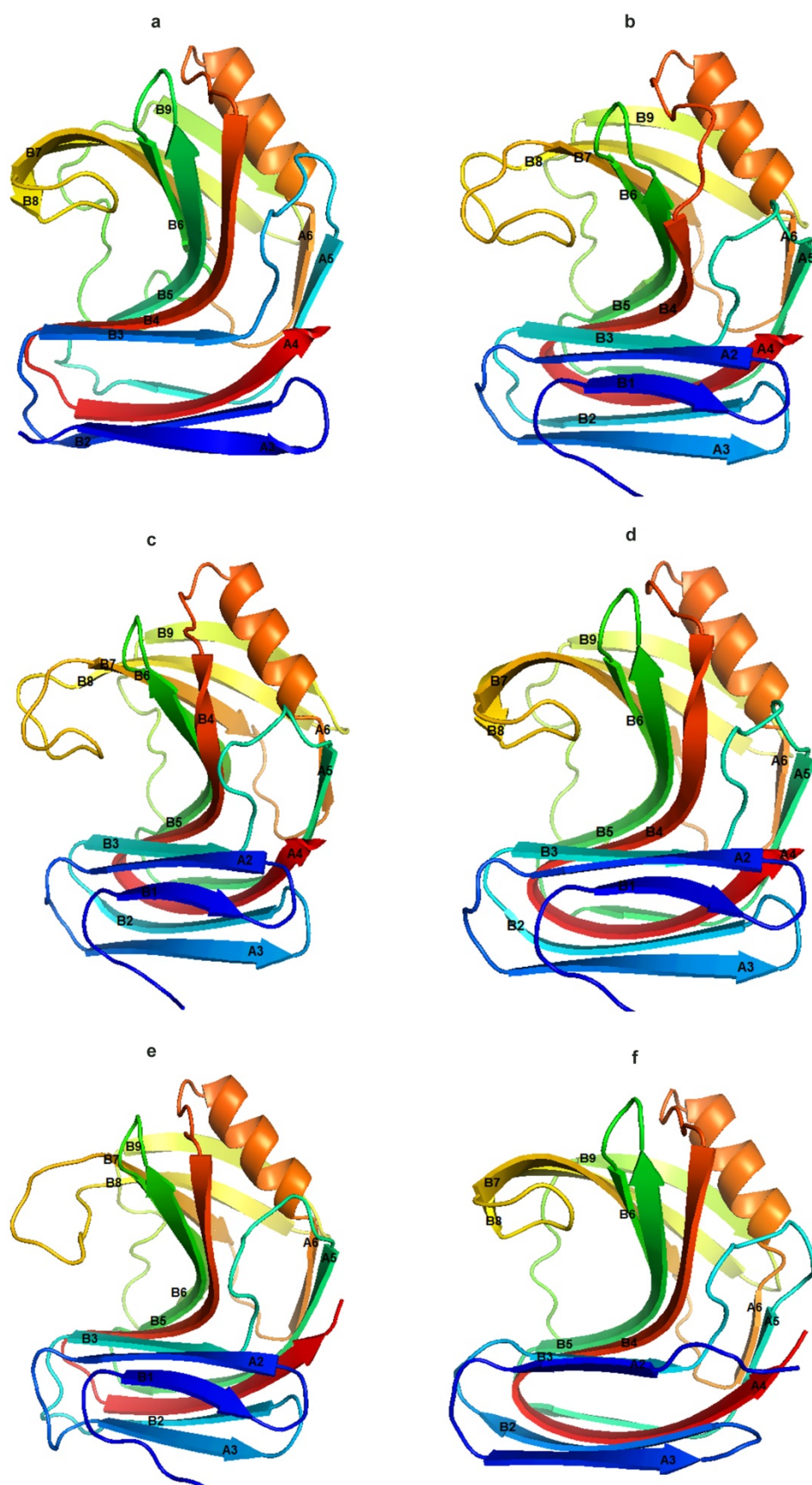
*Figure 4. The predicted three-dimensional model structures of the fungal thermoacidophilic GH11 xylanases.*
*a) GaXyl, b) PzXyl, c) AnXyl, d) CvXyl, e) ArXyl, f) OmXyl.*

Among substrate-binding site residues, three residues (T82, Y112, R157) in *Cv*Xyl, two residues (Y114 and R157) in *Om*Xyl, and two residues (E208 and R153) in *An*Xyl (*Figure 3*) were commonly conserved in the active site of the GH11 xylanases (Paës et al., 2012). These three xylanases had the highest binding efficiency with the substrates (*Table 3*). On the other hand, *Ar*Xyl-docked complexes commonly had interactions between three residues (Y115 in B6-strand, Q159 in B7-strand, I151 in loop between B7-strand and B8-strand) and the substrates. Besides this, three residues in *Ga*Xyl (Q116 in B8-strand, Q130 in B7-strand, Y165 in B4-strand) interacted with two substrates. Also, *Pz*Xyl-docked complexes included polar contacts between three residues (T121 in the loop between B6-strand and B9-strand, Y98 in B5-strand, E200 in B4-strand) and the substrates. Among substrate-binding site residues, three residues (Y115, Q159, and I151) in *Ar*Xyl, two residues (Q116 and Q130) in *Ga*Xyl, and two residues (Y98 and E200) in *Pz*Xyl (*Figure 3*) were commonly conserved in the active site of GH11 xylanase enzymes (Paës et al., 2012). These enzymes (*Ar*Xyl, *Ga*Xyl, and *Pz*Xyl) had relatively lower binding efficiency, compared to the *Cv*Xyl, *Om*Xyl, and *An*Xyl (*Table 3*). Arginine residue in B8-strand was conserved in *Cv*Xyl, *Om*Xyl, and *An*Xyl enzymes. A recent study indicated that this residue in the thermoalkaliphilic GH11 xylanases commonly interacted with the $X_2$-$X_5$ substrates by a higher binding efficiency (Sürmeli, 2022). Also, the replacement of the arginine with asparagine or lysine leads to the activity reduction in *Bacillus circulans* xylanase (Wakarchuk et al., 1994). In addition, arginine was placed in GH11 xylanases at a great prevalence of 88% (Paës et al., 2012). Thus, this study suggests that this conserved arginine residue in B8-strand may play a crucial role in the catalytic action.

***Table 3. The docking analysis scores of the poses with the smallest free energy.***

| No | UniProt ID | Protein name | $X_4$ affinity (kcal/mol) | $X_5$ affinity (kcal/mol) |
|:--:|:--:|:--:|:--:|:--:|
| 1 | A0A6A4H8W9 | *Ga*Xyl | -7.4 | -7.1 |
| 2 | A0A1L9SJU9 | *Pz*Xyl | -7.4 | -8.1 |
| 3 | A0A318YH97 | *An*Xyl | -8.0 | -8.4 |
| 4 | A0A167IM53 | *Cv*Xyl | -9.8 | -8.9 |
| 5 | A0A150VDR5 | *Ar*Xyl | -7.5 | -7.1 |
| 6 | A0A0C3CZX7 | *Om*Xyl | -9.0 | -8.6 |

### 4. Conclusions

The present work had *in silico* analyses of six bacterial thermoacidophilic GH11 xylanases (*Ga*Xyl, *Pz*Xyl, *An*Xyl, *Cv*Xyl, *Ar*Xyl, and *Om*Xyl) to consider their phylogenetic closeness, amino acid sequence resemblance, three-dimensional predicted model structures, and the interactions with the substrates. According to the results, the six GH11 xylanase enzymes might highly have thermoacidophile aspect since they had a high ratio of T/S and NCR/PCR. Also, phylogenetic analysis indicated that the xylanases were clustered into three different parties as first group (*Pz*Xyl, *An*Xyl, and *Cv*Xyl), the second group (*Ga*Xyl and *Om*Xyl), and the third group (*Ar*Xyl). The amino acid alignment results demonstrated that 11 amino acids in the active region of GH11 xylanase enzymes were conserved in the six thermoacidophilic xylanases using *Thermobacillus xylanilyticus* xylanase (Tx-xyl) as a superimposed reference enzyme. The alignment analysis also showed that the five xylanases (*Ar*Xyl, *Om*Xyl, *Cv*Xyl, *Pz*Xyl, *An*Xyl) had greater NTR size, compared to the *Ga*Xyl and Tx-xyl, indicating that they might have higher thermostability. Homology model analysis results indicated that the six enzymes highly possessed similar structural patterns composed of the β-jelly roll domain, which resembles a partially closed right hand. The docking analysis showed that *Cv*Xyl, *Om*Xyl, and *An*Xyl possessed greater binding efficiency with two substrates ($X_4$, and $X_5$), relative to the *Ga*Xyl, *Pz*Xyl, and *Ar*Xyl enzymes. The former three enzymes had the conserved arginine residue in the B8 β-strand involved in the substrate interaction, indicating that it may play a crucial role in their catalytic action. Thus, this study proposed that three thermoacidophilic xylanases (*Cv*Xyl, *Om*Xyl, and *An*Xyl) may be more favorable as the animal feed additive.
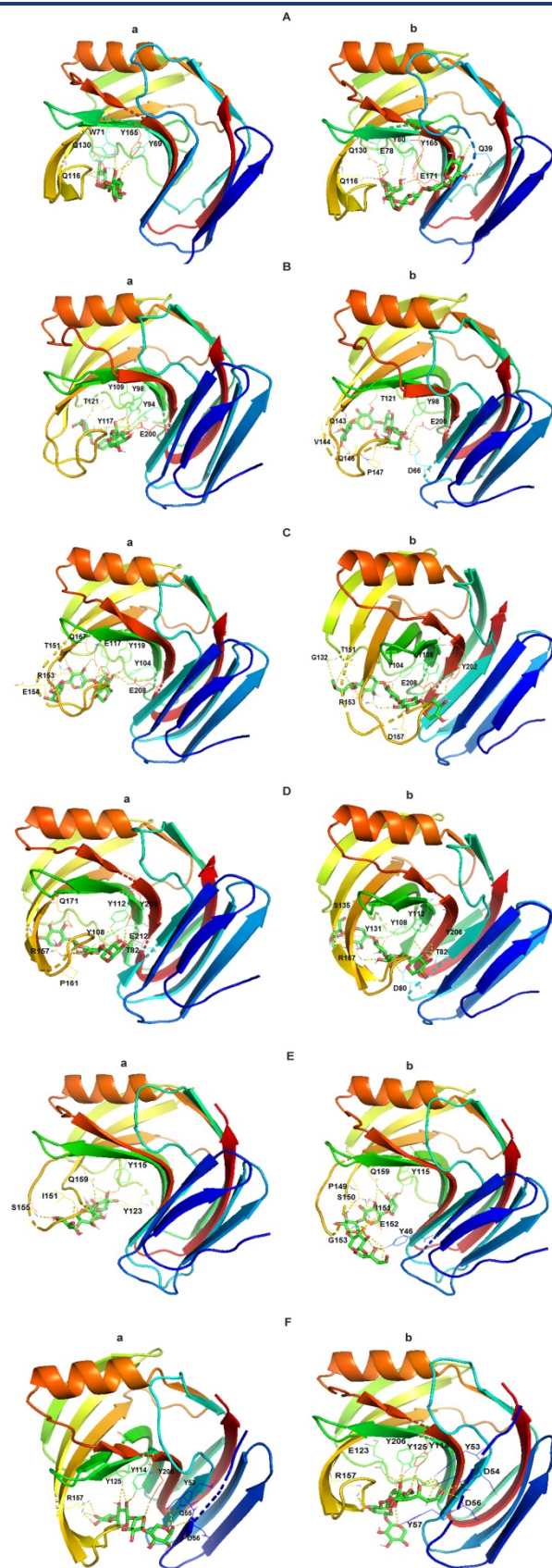
*Figure 5. The interactions between each thermoacidophilic xylanase and the substrates. A) GaXyl, B) PzXyl, C) AnXyl, D) CvXyl, E) ArXyl, F) OmXyl. Left indicates enzyme-docked xylotetraose complexes, and the right indicates enzyme-docked xylopentaose complexes.*

# References

Alagawany, M., Elnesr, S.S., Farag, M.R. (2018). The role of exogenous enzymes in promoting growth and improving nutrient digestibility in poultry. *Iranian Journal of Veterinary Research,* 19(3):157-164.

Algan, M., Sürmeli, Y., Şanlı-Mohamed, G. (2021). A novel thermostable xylanase from *Geobacillus vulcani* GS90: Production, biochemical characterization, and its comparative application in fruit juice enrichment. *Journal of Food Biochemistry,* 45(5): e13716.

Bajpai, P. (1999). Application of enzymes in the pulp and paper industry. *Biotechnology Progress*, 15(2):147–157.

Barbi, F., Kohler, A., Barry, K., Baskaran, P., Daum, C., Fauchery, L., …, Martin, F. (2020). Fungal ecological strategies reflected in gene transcription - a case study of two litter decomposers. *Environmental Microbiology*, 22(3):1089-1103.

Basu, M., Kumar, V., Shukla, P. (2018). Recombinant approaches for microbial xylanases: recent advances and perspectives. *Current Protein & Peptide Science*, 19:87–99.

Başkavak, S., Özdüven, M.L., Polat, C., Koç, F. (2008). The effects of lactic acid bacteria+enzyme mixture silage inoculant on wheat silage. *Journal of Tekirdag Agricultural Faculty,* 5(3):291-296.

Beg, Q.K., Kapoor, M., Mahajan, L., Hoondal, G.S. (2001). Microbial xylanases and their industrial applications: A review. *Applied Microbiology and Biotechnology,* 56(3–4):326–338.

Biely, P., Singh, S., Puchart, V. (2016). Towards enzymatic breakdown of complex plant xylan structures: state of the art. *Biotechnology Advances,* 34:1260–1274.

Boonyapakron, K., Jaruwat, A., Liwnaree, B., Nimchua, T., Champreda, V., Chitnumsub, P. (2017). Structure-based protein engineering for thermostable and alkaliphilic enhancement of endo-β-1,4-xylanase for applications in pulp bleaching. *Journal of Biotechnology*, 259:95–102.

Bowie, J.U., Lüthy, R., Eisenberg, D. (1991). A method to identify protein sequences that fold into a known three-dimensional structure. *Science,* 253(5016):164–170.

Chadha, B.S., Kaur, B., Basotra, N., Tsang, A., Pandey, A. (2019). Thermostable xylanases from thermophilic fungi and bacteria: Current perspective. *Bioresource Technology,* 277:195–203.

Chakdar, H., Kumar, M., Pandiyan, K., Singh, A., Nanjappan, K., …, Srivastava, A.K. (2016). Bacterial xylanases: biology to biotechnology. *3 Biotech*, 6:(2).

Cheng, Y.S., Chen, C.C., Huang, C.H., Ko, T.P., Luo, W., Huang, J.W., …, Guo, R.T. (2014). Structural analysis of a glycoside hydrolase family 11 xylanase from *Neocallimastix patriciarum* : Insights into the molecular basis of a thermophilic enzyme. *Journal of Biological Chemistry,* 289:11020–11028.

Collins, T., Gerday, C., Feller, G. (2005). Xylanases, xylanase families and extremophilic xylanases. *FEMS Microbiology Reviews,* 29(1):3–23.

de Vries, R.P., Riley, R., Wiebenga, A., Aguilar-Osorio, G., Amillis, S., Uchima, C.A., …, Grigoriev, I.V. (2017). Comparative genomics reveals high biological diversity and specific adaptations in the industrially and medically important fungal genus *Aspergillus*. *Genome Biology*, 18(1):28.

Debeire-Gosselin, M., Loonis, M., Samain, E., Debeire, P. (1992). Purification and Properties of a 22 kDa Endoxylanase Excreted by a New Strain of Thermophilic *Bacillus*. In: Visser, J., Beldman, G., van Someren, M. A., Kusters-, Voragen A. G. J., (eds). Xylans and xylanases. Amsterdam, The Netherlands: Elsevier Science Publishers B.V., pp. 463–466.

Decelle, B., Tsang, A., Storms, R.K. (2004). Cloning, functional expression and characterization of three *Phanerochaete chrysosporium* endo-1,4-β-xylanases. *Current Genetics*, 46:166–175.

Deng, P., Li, D., Cao, Y., Lu, W., Wang, C. (2006). Cloning of a gene encoding an acidophilic endo-β-1,4-xylanase obtained from *Aspergillus niger* CGMCC1067 and constitutive expression in *Pichia pastoris*. *Enzyme and Microbial Technology*, 39(5):1096-1102.

Drula, E., Garron. M.-L., Dogan, S., Lombard, V., Henrissat, B., Terrapon, N. (2022). The carbohydrate-active enzyme database: functions and literature. *Nucleic Acids Research,* 50(D1):D571–D577.

Fushinobu, S., Ito, K., Konno, M., Wakagi, T., Matsuzawa, H. (1998). Crystallographic and mutational analyses of an extremely acidophilic and acid-stable xylanase: biased distribution of acidic residues and importance of Asp37 for catalysis at low pH. *Protein Engineering*, 11:1121–1128.

Galanopoulou, A.P., Haimala, I., Georgiadou, D.N., Mamma, D., Hatzinikolaou, D.G. (2021). Characterization of the highly efficient acid-stable xylanase and β-xylosidase system from the fungus *Byssochlamys spectabilis* ATHUM 8891 (*Paecilomyces variotii* ATHUM 8891). *Journal of Fungi*, 7(6):430.

Gasteiger, E., Hoogland. C., Gattiker, A., Duvaud, S., Wilkins, M.R., Appel, R.D., Bairoch, A. (2005). Protein Identification and Analysis Tools on the ExPASy Server. In: Walker, J. M. (eds) The Proteomics Protocols Handbook, Springer Protocols Handbooks, Humana Press.

Hakulinen, N., Turunen, O., Jänis, J., Leisola, M., Rouvinen, J. (2003). Three-dimensional structures of thermophilic β-1,4-xylanases from *Chaetomium thermophilum* and *Nonomuraea flexuosa*. *FEBS Journal,* 270(7):1399–1412.

Han, N., Miao, H., Ding, J., Li, J., Mu, Y., Zhou, J., Huang, Z. (2017). Improving the thermostability of a fungal GH11 xylanase via site-directed mutagenesis guided by sequence and structural analysis. *Biotechnology for Biofuels,* 10:133.

Harris, G.W., Jenkins, J.A., Connerton, I., Cummings, N., Lo, L.L., Scott, M., …, Pickersgill, R.W. (1994). Structure of the catalytic core of the family F xylanase from *Pseudomonas fluorescens* and identification of the xylopentaose-binding sites. *Structure,* 2(11):1107–1116.

Heinig, M., Frishman, D. (2004). STRIDE: a web server for secondary structure assignment from known atomic coordinates of proteins. *Nucleic Acids Research*, 32:W500.

Intasit, R., Cheirsilp, B., Suyotha, W., Boonsawang, P. (2022). Purification and characterization of a highly-stable fungal xylanase from *Aspergillus tubingensis* cultivated on palm wastes through combined solid-state and submerged fermentation. *Preparative Biochemistry & Biotechnology,* 52(3):311-317.

Kataoka, M., Akita, F., Maeno, Y., Inoue, B., Inoue, H., Ishikawa, K. (2014). Crystal structure of *Talaromyces cellulolyticus* (formerly known as *Acremonium cellulolyticus*) GH Family 11 xylanase. *Applied Biochemistry and Biotechnology*, 174:1599–1612.

Koçyiğit, R., Tüzemen, N. (2012). The effect of probiotic plus enzyme on the fattening performance and feed efficiency ratio of brown Swiss young bulls at two different ages. *Journal of Tekirdag Agricultural Faculty,* 9(1): 45-50.

Ku, T., Lu, P., Chan, C., Wang, T., Lai, S., Lyu, P., Hsiao, N. (2009). Predicting melting temperature directly from protein sequences. *Computational Biology and Chemistry*, 33(6):445–450.

Kumar, A., Gautam, A., Dutt, D., Yadav, M., Sehrawat, N., Kumar, P. (2017). Applications of Microbial Technology in Pulp and Paper Industry. ln: Kumar, A., Dutt, D., Yadav, M. (eds), Microbiology and Biotechnology for a Sustainable Environment, 1st edn, Nova Science Publishers, New York, pp 185-206.

Lao, N.T., Schoneveld, O., Mould, R.M., Hibberd, J.M., Gray, J.C., Kavanagh, T.A. (1999). An *Arabidopsis* gene encoding a chloroplast-targeted beta-amylase. *The Plant Journa,l* 20(5):519–527.

Laskowski, R.A., Rullmann, J.A.C., MacArthur, M.W., Kaptein, R., Thornton, J.M. (1996). AQUA and PROCHECK-NMR: Programs for checking the quality of protein structures solved by NMR. J*ournal of Biomolecular NMR,* 8(4):477–486.

Li, Z., Zhang, X., Li, C., Kovalevsky, A., Wan, O. (2020). Studying the role of a single mutation of a family 11 glycoside hydrolase using high-resolution x-ray crystallography. *The Protein Journal*, 39:671–680.

Liao, H., Xu, C., Tan, S., Wei, Z., Ling, N., Yu, G., …, Xu, Y. (2012). Production and characterization of acidophilic xylanolytic enzymes from *Penicillium oxalicum* GZ-2. *Bioresource Technology,* 123:117-124.

Madeira, F., Park, Y.M., Lee, J., Buso, N., Gur, T., Madhusoodanan, N., …, Lopez, R. (2019). The EMBL-EBI search and sequence analysis tools APIs in 2019. *Nucleic Acids Research,* 47(W1):W636–W641.

Mirdita, M., Von Den Driesch, L., Galiez, C., Martin, M.J., Soding, J., Steinegger, M. (2017). Uniclust databases of clustered and deeply annotated protein sequences and alignments. *Nucleic Acids Research*, 45(D1):D170–D176.

Mosier, A.C., Miller, C.S., Frischkorn, K.R., Ohm, R.A., Li, Z., LaButti, K, …, Banfield, J.F. (2016). Fungi contribute critical but spatially varying roles in nitrogen and carbon cycling in acid mine drainage. *Frontiers in Microbiology*, 7:238.

Motta, F.L., Andrade, C.C.P., Santana, M.H.A. (2013). A Review of Xylanase Production by the Fermentation of Xylan: classification, Characterization and Applications. ln Chandel, A.K., Da Silva, S.S. (eds) Sustainable Degradation of Lignocellulosic Biomass - Techniques, Applications and Commercialization, IntechOpen, London.

Nagy, L.G., Riley, R., Tritt, A., Adam, C., Daum, C., Floudas, D., …, Hibbett, D.S. (2016). Comparative genomics of early-diverging mushroom-forming fungi provides insights into the origins of lignocellulose decay capabilities. *Molecular Biology and Evolution*, 33(4):959-970.

Nordberg Karlsson, E., Schmitz, E., Linares-Pastén, J.A., Adlercreutz, P. (2018). Endo-xylanases as tools for production of substituted xylooligosaccharides with prebiotic properties. *Applied Microbiology and Biotechnology*, 102(21):9081–9088.

Paës, G., Berrin, J.G., Beaugrand, J. (2012). GH11 xylanases: structure/function/properties relationships and applications. *Biotechnol Advances*, 30(3):564–592.

Pai, C.K., Wu, Z.Y., Chen, M.J., Zeng, Y.F., Chen, J.W., Duan, C.H., …, Liu, J.R. (2010). Molecular cloning and characterization of a bifunctional xylanolytic enzyme from *Neocallimastix patriciarum*. *Applied Microbiology and Biotechnology,* 85:1451–1462.

Park, J., Carey, J.B. (2019). Dietary enzyme supplementation in duck nutrition: a review. *Journal of Applied Poultry Research*, 28(3):587-597.

Ravindran, V. (2013). Feed enzymes: the science, practice, and metabolic realities. *Journal of Applied Poultry Research*, 22(3):628-636.

Sánchez, Ó.J., Cardona, C.A. (2008).Trends in biotechnological production of fuel ethanol from different feedstocks. *Bioresource Technology,* 99(13):5270–5295.

Smeets, N., Nuyens, F., Niewold, T., Van Campenhout, L. (2014). Temperature resistance of xylanase inhibitors and the presence of grain-associated xylanases affect the activity of exogenous xylanases added to pelleted wheat-based feeds. *Cereal Chemistry,* 91:572-577.

Steinegger, M., Meier, M., Mirdita, M., Vöhringer, H., Haunsberger, S.J., Söding, J. (2019). HH-suite3 for fast remote homology detection and deep protein annotation. *BMC Bioinformatics,* 20(1):1–15.

Studer, G., Rempfer, C., Waterhouse, A.M., Gumienny, R., Haas, J., Schwede, T. (2020). QMEANDisCo—distance constraints applied on model quality estimation. *Bioinformatics,* 36(8):2647–2647.

Studer, G., Tauriello, G., Bienert, S., Biasini, M., Johner, N., Schwede, T. (2021). ProMod3-A versatile homology modelling toolbox. *PLoS Computational Biology*, 17(1).

Subramaniyan, S., Prema, P. (2002). Biotechnology of microbial xylanases: enzymology, molecular biology, and application. *Critical Reviews in Biotechnology*, 22(1):33–64.

Sürmeli, Y. (2022). Comparative investigation of bacterial thermoalkaliphilic GH11 xylanases at molecular phylogeny, sequence and structure level. *Biologia*, 77:3241–3253.

Tamura, K., Stecher, G., Kumar, S. (2021). MEGA11: molecular evolutionary genetics analysis version 11. *Molecular Biology and Evolution*, 38(7):3022–3027.

The UniProt Consortium. (2021). UniProt: the universal protein knowledgebase in 2021. *Nucleic Acids Research*, 49(D1):D480–D489.

Törrönen, A., Harkki, A., Rouvinen, J. (1994). Three-dimensional structure of endo-1,4-beta-xylanase II from *Trichoderma reesei*: two conformational states in the active site. *The EMBO Journal,* 13(11):2493.

Törrönen, A., Rouvinen, J. (1995). Structural comparison of two major endo-1,4-xylanases from *Trichoderma reesei*. Biochemistry, 34(3):847-856.

Trott, O., Olson, A.J. (2010). AutoDock Vina: improving the speed and accuracy of docking with a new scoring function, efficient optimization and multithreading. *Journal of Computational Chemistry*, 31(2):455.

Turunen, O., Etuaho, K., Fenel, F., Vehmaanperä, J., Wu, X., Rouvinen, J., Leisola, L. (2001). A combination of weakly stabilizing mutations with a disul fide bridge in the α-helix region of *Trichoderma reesei* endo-1,4 -β -xylanase II increases the thermal stability through synergism. *Journal of Biotechnology*, 88:37–46.

Wakarchuk, W.W., Robert, L., Campbell, R.L., Sung, W.L., Davoodi, J., Yaguchi, M. (1994). Mutational and crystallographic analyses of the active site residues of the *Bacillus circulans* xylanase. *Protein Science*, 3:467–475.

Wang, S., Li, W., Liu, S., Xu, J. (2016). RaptorX-Property: a web server for protein structure property prediction. *Nucleic Acids Research*, 44(W1):W430-W435.

Wang, X., Ma, R., Xie, X., Liu, W., Tu, T., Zheng, F., …, Luo, H. (2017). Thermostability improvement of a T*alaromyces leycettanus* xylanase by rational protein engineering. *Scientific Reports*, 7(1):1–9.

Wiederstein, M., Sippl, M.J. (2007). ProSA-web: interactive web service for the recognition of errors in three-dimensional structures of proteins. N*ucleic Acids Research*, 35(suppl_2):W407–W410.

Wood, T.M., McCrae, S.I., Bhat, K.M. (1989). The mechanism of fungal cellulase action. Synergism between enzyme components of *Penicillium pinophilum* cellulase in solubilizing hydrogen bound-ordered cellulose. *Biochemical Journal*, 260(1):37–43.

Xia, T., Wang, Q. (2009). Directed evolution of *Streptomyces lividans* xylanase B toward enhanced thermal and alkaline pH stability. *World Journal of Microbiology and Biotechnology,* 25(1):93–100.

Xiong, H., Fenel, F., Leisola, M., Turunen, O. (2004). Engineering the thermostability of *Trichoderma reesei* endo-1,4- β-xylanase II by combination of disulphide bridges. *Extremophiles*, 8:393–400.

Yi, Y., Xu, S., Kovalevsky, A., Zhang, X., Liu, D., Wan, Q. (2021). Characterization and structural analysis of a thermophilic GH11 xylanase from compost metatranscriptome. *Applied Microbiology and Biotechnology*, 105:7757–7767.

# Supplementary Material

> *Neocallimastix patriciarum* xylanase (UniProt ID: **B8YG19**)
MRLGVALSTIAVLLTATSARNLDKRQWGWPNFGGGNGGNGGNGGKTINDYKREQGAGRDIHVYAPSNLAPNSPLL
LSLHGMDQDPNYQQSNTHWETLADSEGFVVVYPRGGTGMSTWDIQGTKDTQWVSQIIDQMKKEYNIDTKRVYLSG
FSMGGMFTYHAMSQIANKIAAFAPCSGPNVFGASKAQRPVPIFHVHGTNDDVLNYQQVEGFLKNYRDQFHCPSQA
DTKTNYPNRENPNATLYTWGPCDKGVYIKHLKLQGRGHSPSSADIQDIWDFVSQWTVDGPVSASGNGGGNTTPTN
PSTGGNGNGNGGGNTTPTNPSTGGNGNGNGGSTDKCSSNITKQGYKCCASNCEVVYTDSDGDWGVENDQWCGCGN
RVTVGSGTCSAKILQQGYKCCPSGCIIYYTDEDGTWGVNGEEWCGCGSGSSSTGGGNDAPSSGSGSYQGANGTNFC
NNAKHSGESVTVTSNKVGDINGIGYELWADSGNNSATFYDDGSFSCSFQRAKDYLCRSGLSFDSTKTHKQIGHIY
AEFKLVKQNIQNVDYSYVGIYGWTRNPLVEFYVVDNWLSQWRPGDWVGNKKHGDFTIGGAQYTVYENTRYGPSID
GDTNFKQYFSIRQQPRDCGTIDITAHFEQWEKLGMTMGKMHEAKVLGEAGSNNGGTSGTADFPFAKVYVKN


> *Aspergillus niger* xylanase B(UniProt ID: P55330)
MLTKNLLLCFAAAKAALAVPHDSVAQRSDALHMLSERSTPSSTGENNGFYYSFWTDGGGDVTYTNGDAGAYTVEW
SNVGNFVGGKGWNPGSAQDITYSGTFTPSGNGYLSVYGWTTDPLIEYYIVESYGDYNPGSGGTYKGTVTSDGSVY
DIYTATRTNAASIQGTATFTQYWSVRQNKRVGGTVTTSNHFNAWAKLGMNLGTHNYQIVATEGYQSSGSSSITVQ


> *Penicillium oxalicum* xylanase B (UniProt ID: E7EF85)
MISLSSVAIALTTVVGALALPSDQSVNLAARQAITSSQTGTNNGYYYSFWTNGAGSVSYSNGAAGQFSVNWANQG
GGDFTCGKGWNPGKAQDISFSGTFTPNGNAYLSIYGWTTGPLVEYYILENFGSYNPGNGMTHVGTLTSDGSDYDI
YKHTQVNQPSIVGTSTFDQYWSIRKNKRSSGTVTTANHFSAWASHGMNLGSHNYQILSVEGYQSSGSASMTVSAG
SSSSGGSGSGSGSGSGSGSGSGSGSGSQTTTAGSSTGTGTGSGSGSGSGGSGGNCAAQWGQCGGQGWNGPTCCSSGTCK
ASNQWYSQCL


> *Phanerodontia chrysosporium* xylanase B(UniProt ID: B7SIW1)
MVSFNSLLVAVSAATCALAFPFEFHNGTHVFPRQSTPAGTGTNNGYFYSFWTDGGGSVTYNNGPAGEYSVTWSNA
DNFVAGKGWNPGSAQAISFTANYQPNGNSYLSVYGWSTNPLVEYYILEDFGTYNPAVSLTHKGTLTSDGATYDVY
EGTRVNEPSIQGTATFNQYWSIRSSKRSSGTVTTANHFAAWKQLGLPLGTFNYQIVATEGYQSSGSSTVTVNPAG
GVTSPIAPTGPSSVSTTPSGPSSSPSPVGTCSALYGQCGGQGWTGPTCCSSGTCKFSNNWYSQCL


*Figure S1. Amino acid sequences of four biochemically characterized GH11 xylanase enzymes. These enzymes were compared with the six fungal thermoacidophilic GH11 xylanases in this study for NCR/PCR and T/S ratios.*
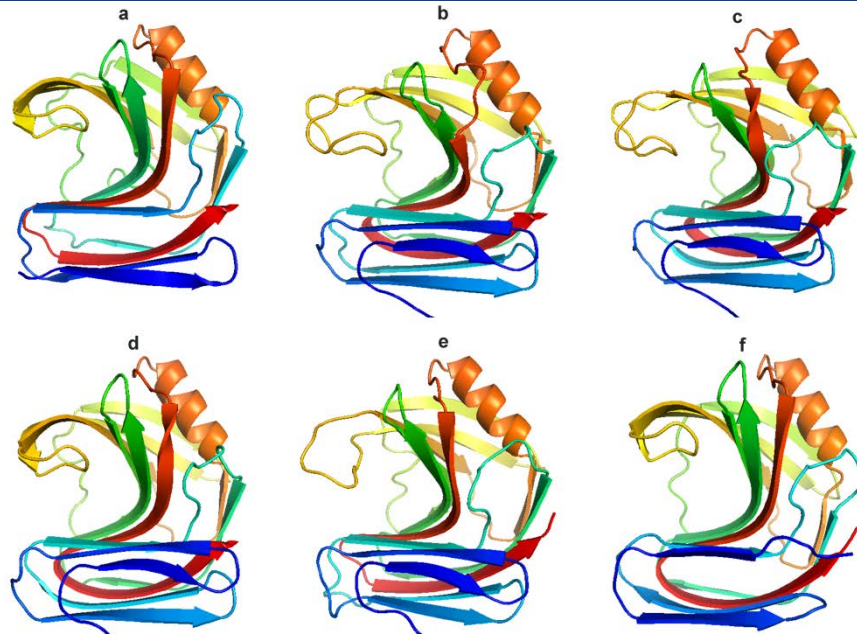
*Figure S2. The predicted model structures of the six fungal thermoacidophilic GH11 xylanases by SWISS-MODEL. a) GaXyl, b) PzXyl, c) AnXyl, d) CvXyl, e) ArXyl, f) OmXyl*
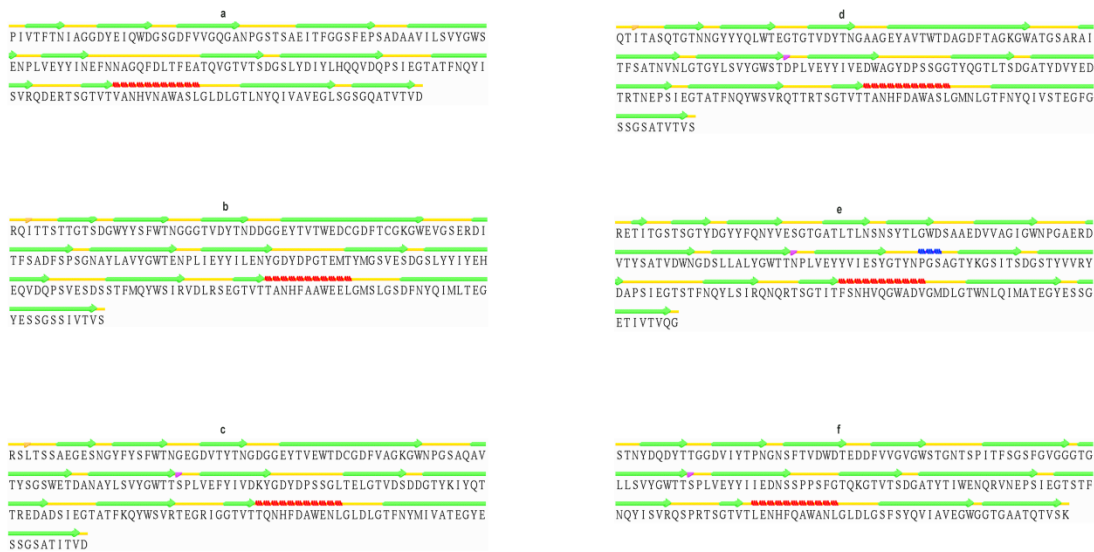


*Figure S3. The secondary structure of the predicted model structures of six fungal thermoacidophilic GH11 xylanases evaluated by Stride. a) GaXyl, b) PzXyl, c) AnXyl, d) CvXyl, e) ArXyl, f) OmXyl*
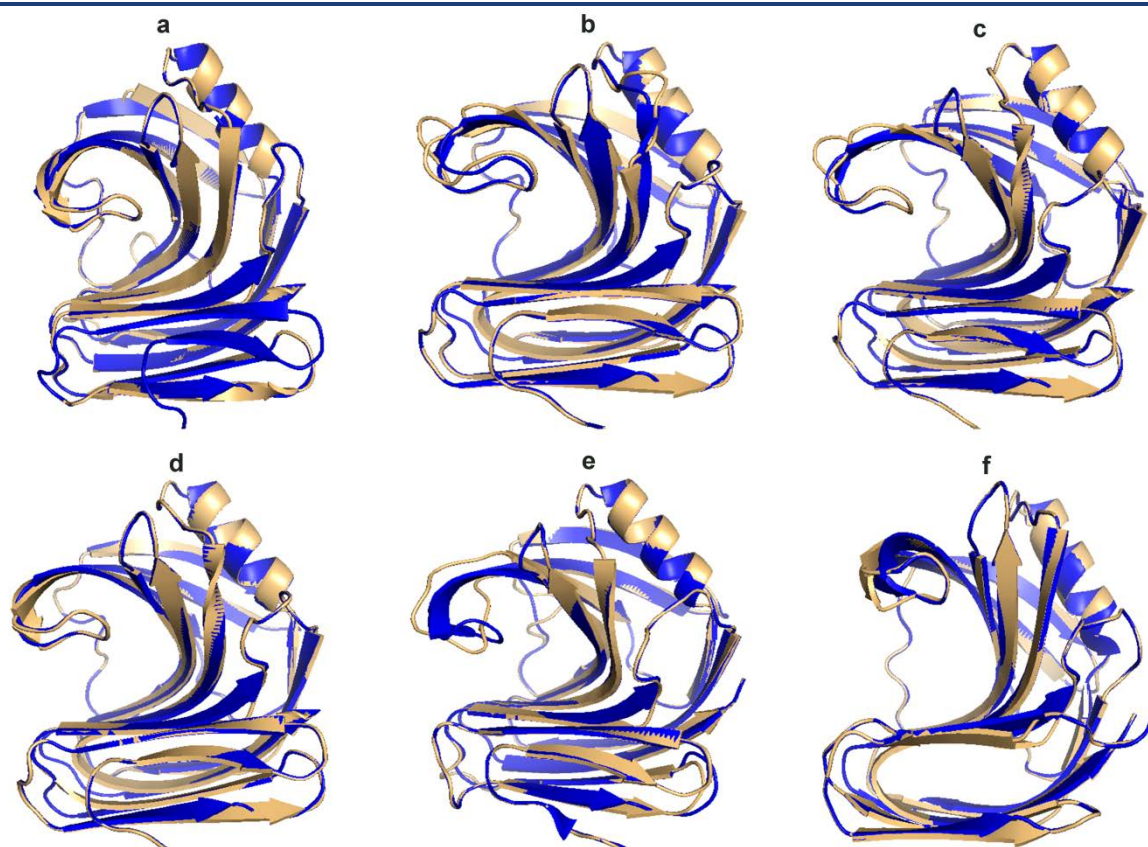
*Figure S4. The model-template structural alignment monitored by PyMOL. a) GaXyl, b) PzXyl, c) AnXyl, d) CvXyl, e) ArXyl, f) OmXyl. Blue refers to template, and light orange indicates to the each thermoacidophilic xylanase*
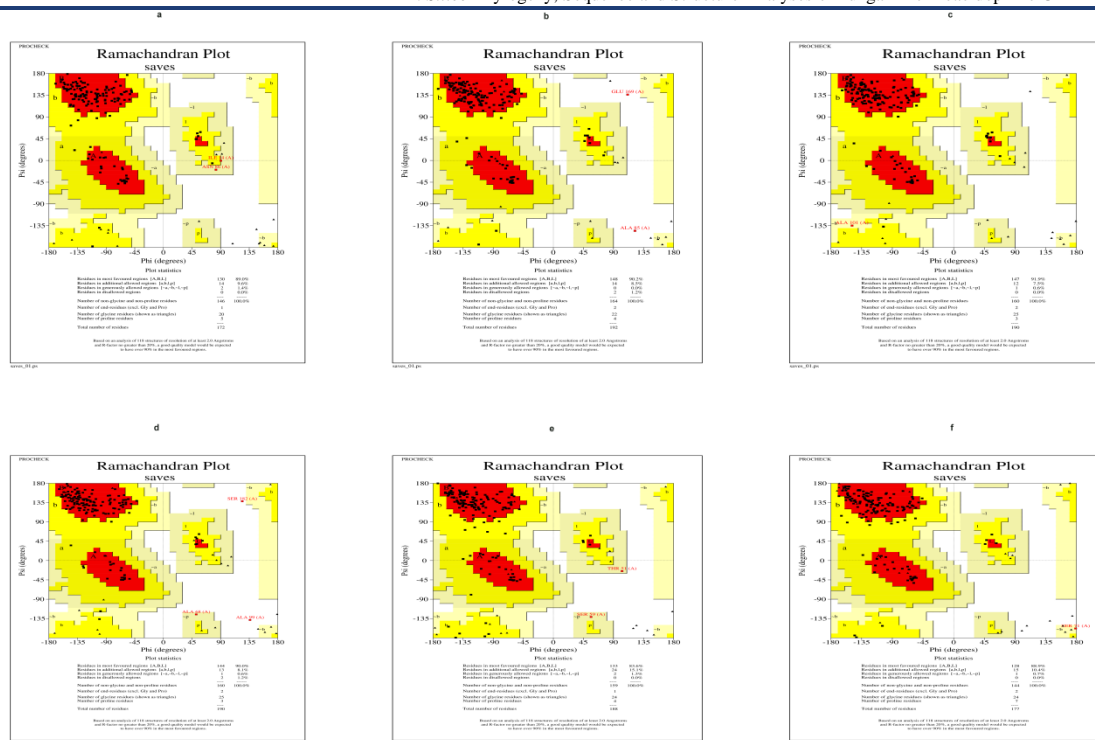
*Figure S5. Ramachandran plots of the six fungal thermoacidophilic GH11 xylanases estimated using ProCheck. a) GaXyl, b) PzXyl, c) AnXyl, d) CvXyl, e) ArXyl, f) OmXyl.*
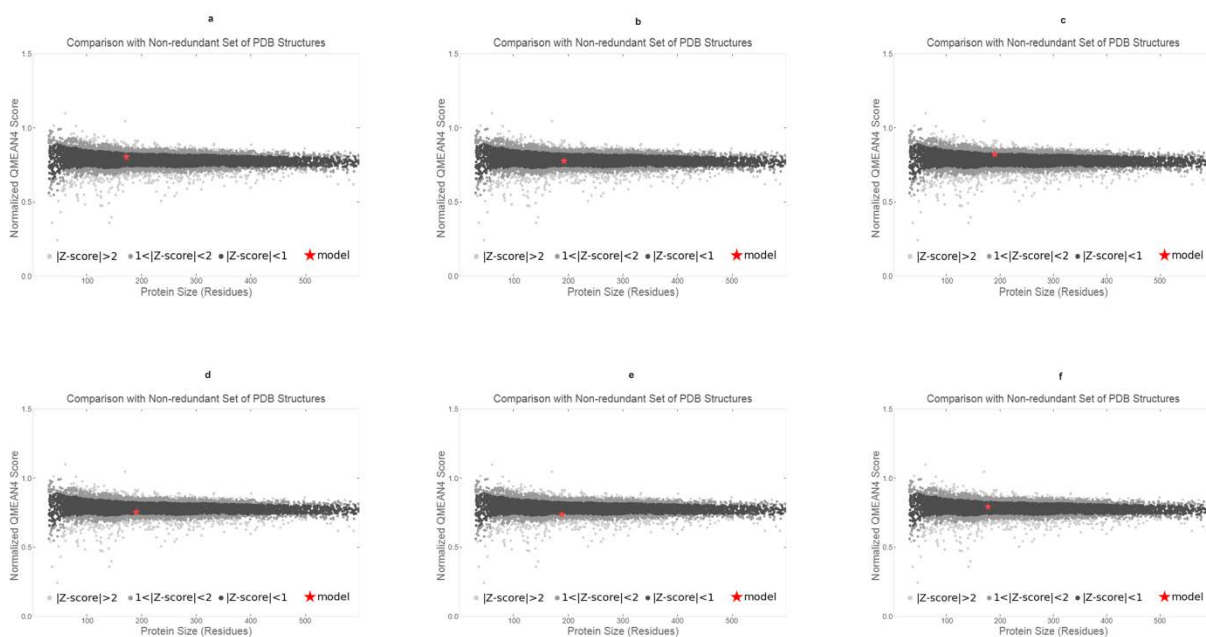


*Figure S6. QMEAN value of the six fungal thermoacidophilic GH11 xylanases.*

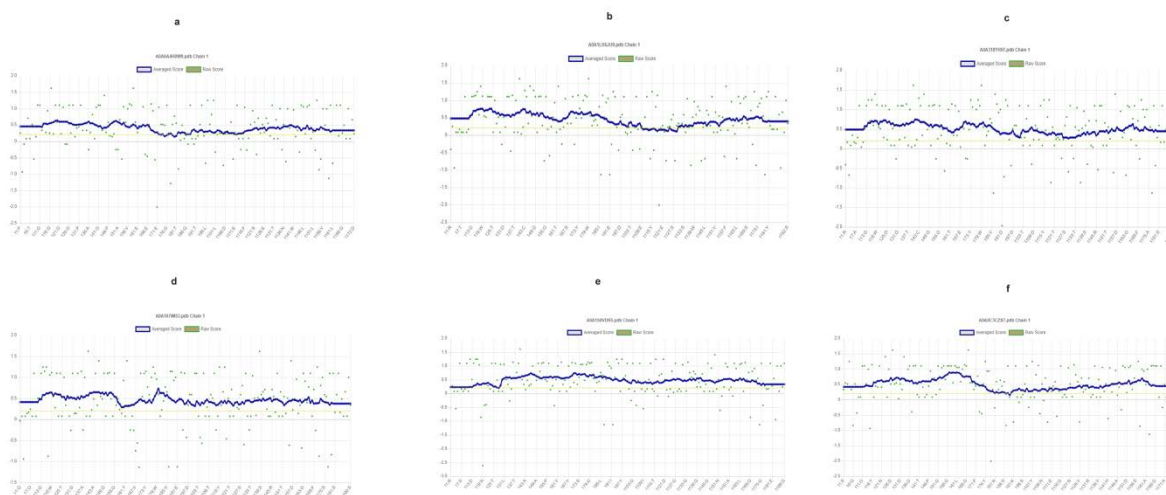*a) GaXyl, b) PzXyl, c) AnXyl, d) CvXyl, e) ArXyl, f) OmXyl.*

*Figure S7. Verify 3D assessment for compatibility of the each predicted model of the six fungal thermoacidophilic GH11 xylanases. a) GaXyl, b) PzXyl, c) AnXyl, d) CvXyl, e) ArXyl, f) OmXyl.*
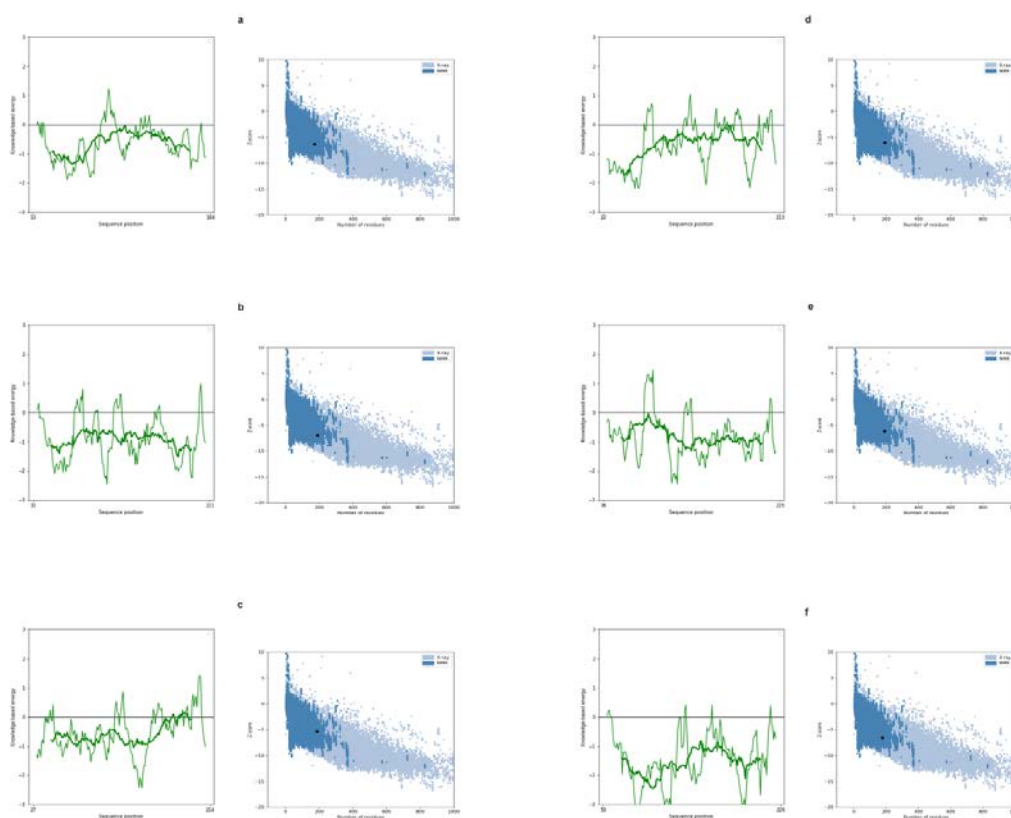


*Figure S8. The global (right) and the local (left) quality of the each predicted model of the six fungal thermoacidophilic GH11 xylanases by ProSA. a) GaXyl, b) PzXyl, c) AnXyl, d) CvXyl, e) ArXyl, f) OmXyl.*